

Sparsity-based Convolutional Kernel Network for Unsupervised Medical Image Analysis

Euijoon Ahn, *Student Member, IEEE*, Jinman Kim, *Member, IEEE*, Ashnil Kumar, *Member, IEEE*, Michael Fulham, and Dagan Feng, *Fellow, IEEE*

Abstract—The availability of large-scale annotated image datasets coupled with recent advances in supervised deep learning methods are enabling the derivation of representative image features that can potentially impact different image analysis problems. However, such supervised approaches are not feasible in the medical domain where it is challenging to obtain a large volume of labelled data due to the complexity of manual annotation and inter- and intra-observer variability in label assignment. Algorithms designed to work on small annotated datasets are useful but have limited applications. In an effort to address the lack of annotated data in the medical image analysis domain, we propose an algorithm for hierarchical unsupervised feature learning. Our algorithm introduces three new contributions: (i) we use kernel learning to identify and represent invariant characteristics across image sub-patches in an unsupervised manner; (ii) we leverage the sparsity inherent to medical image data and propose a new sparse convolutional kernel network (S-CKN) that can be pre-trained in a layer-wise fashion, thereby providing initial discriminative features for medical data; and (iii) we propose a spatial pyramid pooling framework to capture subtle geometric differences in medical image data. Our experiments evaluate our algorithm in two common application areas of medical image retrieval and classification using two public datasets. Our results demonstrate that the medical image feature representations extracted with our algorithm enable a higher accuracy in both application areas compared to features extracted from other conventional unsupervised methods. Furthermore, our approach achieves an accuracy that is competitive with state-of-the-art supervised CNNs.

Index Terms—Unsupervised Feature Learning, Medical Image Retrieval, Medical Image Classification, Convolutional Neural Network, Transfer Learning.

I. INTRODUCTION

Some form of medical imaging is now ubiquitous in everyday healthcare for diagnosis, staging the extent of disease, treatment planning, and assessing response to therapy. There are now large image archives that provide new opportunities for evidence-based diagnosis, physician training and biomedical research [1]. Hence there has been great interest in computer-aided diagnosis (CAD) systems that can

automatically analyse, categorise or retrieve images. These CAD systems often relate low-level image features to high-level semantic concepts or expert domain knowledge using machine learning techniques.

Learning-based algorithms take advantage of the incorporation of prior knowledge derived from labelled training data. Deep learning approaches, such as convolutional neural networks (CNNs), produce impressive results in natural (photographic) image classification [2],[3],[4]. CNNs learn image features in a hierarchical fashion. Each deeper layer of the network learns a representation of the image data that is semantically more meaningful, e.g., in a classification application the learned features can be a class-specific representation [5] that enables better discrimination between different image classes [2],[3]. CNNs require a large number of annotated training images (e.g., ImageNet with over 1 million natural images). In the medical imaging domain, however, there is a limited availability of large annotated datasets; medical images are complex to interpret, requiring clinicians to label the images, which is a costly exercise that is further hindered by inter- and intra-observer variability among clinicians [6].

The concept of transfer learning has been used to overcome the lack of available labelled medical image data, either by using a model that was pre-trained on a different domain (e.g., natural images [7]) as a generic feature extractor, or alternatively, using a relatively small set of medical images to optimise a pre-trained model from a different domain (i.e., fine-tuning) [8],[9],[10],[11]. Unfortunately, since these approaches rely upon more general image features they may potentially be unable to capture the high-level semantic features that are most relevant for a specific dataset. Consequently, they are unable to match the overall accuracy of learning image features directly from large annotated data of a specific type. An emerging approach to tackle this limitation is to use unsupervised feature learning algorithms to build features from unlabelled data, which allows large unannotated medical image collections to be used. Many of these approaches are based on algorithms such as sparse coding [12], sparse auto-encoders [13], and Restricted Boltzmann Machines (RBMs) [14]. However, many of these methods have only shown strong performance in learning low-

E. Ahn, J. Kim, A. Kumar, and D. Feng are with the School of Information Technologies, University of Sydney, NSW, Australia. E. Ahn (E-mail: eahn4614@uni.sydney.edu.au); J. Kim (E-mail: jin-man.kim@sydney.edu.au); A. Kumar (E-mail: ashnil.kumar@sydney.edu.au).

M. Fulham is with the Department of Molecular Imaging, Royal Prince Alfred Hospital, Camperdown, NSW, Australia, and also with the Sydney

Medical School, University of Sydney, Camperdown, NSW, Australia (E-mail: michael.fulham@sydney.edu.au).

D. Feng is also with Med-X Research Institute, Shanghai Jiao Tong University, China (E-mail: Dagan.feng@sydney.edu.au).

The research was funded in part by Australia Research Council grants.

level features such as ‘blobs’ or ‘edges’. Only a few methods have succeeded in extracting semantic high-level features, such as the stacked sparse autoencoder (SSAE) presented by Le et al. [5], which learned image features in a hierarchical manner. The SSAE was used to pre-train a model that was later coupled to supervised deep learning (i.e., fine-tuning) and achieved improved results in object recognition [5]; the unsupervised pre-training learned useful priors that acted as an initialisation point for the supervised fine-tuning, making the supervised model less prone to overfitting or being trapped in local minima [15],[16].

Hierarchical convolutional kernel-based networks (CKNs) have recently been introduced to generate multi-layer image representations in an unsupervised manner [17], with state-of-the-art performance in natural image classification [17] and retrieval [18]. The CKN architecture is capable of learning the local geometry of the data without reliance on labels. The kernel learning is a function that describes an inner product of any two training samples in some induced Hilbert space [19]. It formalises the notion of similarity and provides a representation of the data that can better reconstruct training samples. CKNs incorporate these characteristics and learn data representations in a non-linear hierarchical manner. However, they are prone to overfitting when the number of training data is small. That is, the learning cost function often gets stuck in local minima.

The concept of sparsity has been widely used in computer vision and has proven to be effective in image compression [20], denoising [21], and tomographic reconstructions. Sparsity can be used to derive compact and optimal representations of image data, where a number of trivial information or parameters can be ignored without compromising image quality or characteristics [22]. For example, the temporal resolution of magnetic resonance (MR) imaging was greatly improved [23] with the use of an additional sparsity constraint, thereby allowing for the development of a number of novel CAD systems in cardiac and brain imaging. Our hypothesis is that if we use such sparsity constraints, we will potentially enable the derivation of compact and optimal representations of medical images.

In this paper, we propose a new sparse convolutional kernel network (S-CKN) that leverages the sparsity inherent to medical image data to address the current limitations outlined above. Our S-CKNs can be pre-trained in a layer-wise fashion to extract sparse features that are more relevant to medical image data, i.e., are more discriminative for medical images. In addition, we couple our S-CKN to a spatial pyramid pooling (SPP) framework that enables a better characterisation of the local geometry of the medical image data. We validate our proposed method on two public datasets with comparisons to other unsupervised feature learning algorithms as well as supervised CNNs. The main contributions of our work can be summarized as follows:

- 1) A new approach to characterise medical images by combining kernel learning and CNNs to learn the local geometry of the medical data in a hierarchical manner.
- 2) An unsupervised sparse feature learning algorithm which effectively learns initial discriminative features. Specifically,

the algorithm is used to initialise the weights of a CKN, which can be pre-trained in a layer-wise fashion. We emphasize that our proposed method is completely unsupervised, which is more challenging than the standard use of supervised CNNs.

- 3) A spatial pyramid pooling framework that provides more discriminative and geometrically invariant local feature representations of medical image data.

- 4) A comprehensive comparison of our approach to state-of-the-art methods.

II. RELATED WORK

A. X-ray Image Retrieval

Plain X-ray images are commonly performed and well-understood medical images. The retrieval of X-ray image is a critical step for imaging-based clinical decision support systems [24],[25],[7]. Automated X-ray image retrieval, however, is challenging due to irregular brightness and contrast, and artifacts caused by prostheses and other implants. There are also high intra-class variability and inter-class similarity among images in X-ray repositories.

Prior studies have used hand-crafted descriptors and as such the similarity of classes was only measured within the specific feature space. Moreover, these features were often represented as a collection of unordered local features and disregarded the local geometry of the features. For example, the scale-invariant feature transform (SIFT) was used to extract image features invariant to changes in scaling orientation and illumination and coupled with the bag-of-visual words (BoVW) model to form a histogram representation of the image [26, 27]. Other common approaches used a combination of multi-visual features including local binary patterns, texture and shape [28]. Avni et al. [26] presented densely sampled normalised features coupled with spatial information for X-ray categorisation and retrieval.

Anavi et al. [29] recently benchmarked hand-crafted descriptors against features extracted using pre-trained CNNs, and concluded that the pre-trained CNNs produced state-of-the-art results for chest X-ray classification. Recently, Ahn et al. [7] combined hand-crafted local features with learned features transferred from a different domain. However, as mentioned previously, such features cannot currently match the overall accuracy of directly learning features from a large dataset that is specific to the problem domain [9, 10].

B. Medical Imaging Modality Classification

While a multitude of different types of images have been collected to assist in the development of more advanced CAD systems, the labelling of the collated image data remains problematic [30],[31],[32],[33]. In cases where appropriate labels are absent, automatic identification of the imaging modality is an initial important step because the semantics and content of an image can vary greatly depending on the modality.

In prior research, a variety of algorithms have been used to extract and fuse a range of image features [34]. These features were often designed by humans to derive particular underlying image characteristics such as colour, texture, local binary patterns, and spatial orientation. The performance of these algorithms was limited by the quality of the features. Kumar et

al. recently proposed an ensemble of fine-tuned CNNs to learn different levels of semantic image representations [8].

III. METHODS

A. Background: Convolutional Neural Networks

CNNs process an input image using multiple layers and learn features in a hierarchical manner. CNN layers generally have: 1) convolutional layers to learn weights (i.e., filters) that can be used to extract features from the input; 2) a linear operation followed by a pointwise non-linearity such as Sigmoid or rectified linear units, which prevents explosion of gradients and speeds up training; and 3) pooling layers to aggregate features that are in spatial proximity (down-sampling the data in the process). The output of single layer CNN can be represented as:

$$f(\mathbf{O}) = \text{pool}_p(\sigma(W \otimes \mathbf{O} + \mathbf{b})), \quad (1)$$

where \mathbf{O} is the input feature vector, $\sigma(\cdot)$ is the pointwise non-linear function and $\theta = \{W, \mathbf{b}\}$ are the set of parameters (i.e., weights and biases). The pool function denotes a down-sampling operation and p is the size of pooling region. The symbol \otimes indicates the linear convolution. When a convolutional layer is dense and unstructured, it is called “fully connected”. For example, the well-established AlexNet [35] CNN has 8 trainable layers comprising five convolutional layers followed by three fully connected layers. Training such a CNN, however, is challenging because of the number of hyperparameters that need to be carefully tuned. Some major hyperparameters include the size of learnable filters, the number of layers, the number of outputs per layer, and the size of the down-sampling factor. Sub-optimal hyperparameter choice leads to overfitting and an inability to derive optimal high-level semantic image features. Some supervised CNNs have exploited unsupervised layerwise pre-training schemes to render better generalisation of image data [5],[16]. The pre-training acts as a form of regularisation which minimises variance and restricts the range of the parameter values for subsequent supervised training [15]. Layerwise unsupervised pre-training allows all the available unlabelled image data to be used to pre-train the network’s local parameters, which

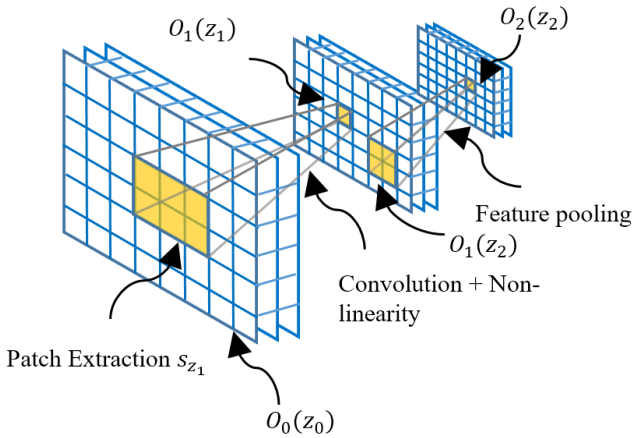


Fig 1. A two-layer convolutional kernel network; each layer is a weighted match kernel between all sub-patches of the previous layer.

potentially provides a good initialisation point for further supervised training.

B. Convolutional Kernel Networks

CKNs have the classic hierarchical architecture of CNNs but use kernel maps to represent image features. A kernel map is used to understand the local geometry of the image data by modelling invariance [17]. We suggest that kernels coupled with a hierarchical architecture allow the effective learning of image features without a reliance on labels. The architecture of a two-layer CKN is shown in Fig 1.

Let us consider two image patches O and O' of an image of size $m \times m$ ($m = 200$ in this paper), with Ω being a set of pixel coordinates ($\Omega = \{1, \dots, m\}^2$). Given the location z in Ω , and the sub-patches $s_z \in O$ and $s'_z \in O'$ of the image feature map, we now introduce a single layer convolutional kernel network as follows:

$$K(O, O') = \sum_{z, z' \in \Omega} \|s_z\|_{\mathcal{H}} \|s'_z\|_{\mathcal{H}} e^{-\frac{1}{2\beta^2} \|z-z'\|_2^2} e^{-\frac{1}{2\alpha^2} \|s_z-s'_z\|_{\mathcal{H}}^2} \quad (2)$$

The kernel K is a positive definitive kernel that consists of a sum of pairwise comparisons between image features of sub-patches. The $\|\cdot\|_{\mathcal{H}}$ denotes the Hilbertian norm and the term $\|s_z\|_{\mathcal{H}} \|s'_z\|_{\mathcal{H}}$ acts to emphasise spatial and feature similarity (controlled by the exponential terms) for non-small intensity-valued patches. The term $e^{-\frac{1}{2\beta^2} \|z-z'\|_2^2}$ controls spatial distance between z and z' , and $e^{-\frac{1}{2\alpha^2} \|s_z-s'_z\|_{\mathcal{H}}^2}$ measures the feature similarity between sub-patches.

We used two different types of input feature maps;

1) Patch map: the s_z is an image sub-patch size $b \times b$ centred at z . The sub-patch s_z is simply $\mathbb{R}^{b \times b}$ and \tilde{s}_z denotes a contrast-normalised version of the sub-patch.

2) Gradient map: the sub-patch s_z is the two-dimensional gradient of the image at pixel z , which is computed with first-order differences along each dimension. In this formulation, $\|s_z\|_{\mathcal{H}}$ is the gradient intensity and \tilde{s}_z denotes its orientation defined as an angle with $[\cos \theta, \sin \theta]$ [36]. When the input data is in a compact set ($\mathbb{R}^d, d \leq 2$), Equation (2) can be approximated by uniform sampling over a large enough set; the term $e^{-\frac{1}{2\beta^2} \|z-z'\|_2^2}$ indicates a spatial kernel and $e^{-\frac{1}{2\alpha^2} \|s_z-s'_z\|_{\mathcal{H}}^2}$ denotes the gradient map.

The coefficients β and α are smoothing Gaussian kernel parameters that control spatial distances between z and z' and the feature closeness between \tilde{s}_z and \tilde{s}'_z in Hilbert space respectively. The corresponding kernel map is formalised as a weighted match kernel between all sub-patches from training samples, which defines a feature representation of the image.

C. Unsupervised Feature Learning via CKNs

Match kernels are expensive to compute when the input data has high dimensionality ($\mathbb{R}^d, d > 2$). The computational complexity also grows quadratically with increasing sample sizes. To prevent the curse of dimensionality, we used a fast approximation approach with finite-dimensional embedding proposed by Marial et al. [17]. For all u and z ,

$$K(O, O') \approx \sum_{u \in \Omega_1} g(u; O)^T g(u; O') \quad (3)$$

where

$$g(u; O) := \sum_{z \in \Omega} e^{-\frac{1}{2\beta^2} \|u-z\|_2^2} h(z; O) \quad (4)$$

and

$$h(z; O) := \|s_z\|_2 \left[\sqrt{b_i} e^{-\frac{1}{\alpha^2} \|W_i - \tilde{s}_z\|_2^2} \right]_{i=1}^{n_1}, \quad (5)$$

where Ω_1 is a subset of Ω , and b and W are learned parameters. This operation can be considered to be similar to a spatial convolution of the feature map followed by a pointwise non-linearity. Since $K(O, O')$ is a sum of the match kernel terms, we can learn to approximate the kernel using training data. The parameters b and W are learned at the sub-patch level by solving an optimisation problem:

$$\min_{W_i, b_i} \sum_{c=1}^n \left(e^{-\frac{\|s_c - \tilde{s}'_c\|_2^2}{2\alpha^2}} - \sum_{i=1}^p b_i e^{-\frac{\|W_i - \tilde{s}_c\|_2^2}{\alpha^2}} - e^{-\frac{\|W_i - \tilde{s}'_c\|_2^2}{\alpha^2}} \right) \quad (6)$$

We randomly selected 400,000 pairs of sub-patches from the training data and used the standard Limited memory Broyden Fletcher Goldfarb Shanno with Bounds (L-BFGS-B) [37] optimiser to solve Equation (6) [17]. The L-BFGS-B requires less parameters and can be superior to the conjugate gradient (CG) or stochastic gradient descent (SGD) in many applications such as image classification [38].

D. Layerwise Unsupervised Pre-training with Sparsity

It has been widely demonstrated that feature representations of medical image data have an intrinsic sparse structure under certain fixed bases (e.g., Fourier) [23, 39]. This intrinsic sparsity often comes in two complementary forms [40]: population and lifetime sparsity. Population sparsity refers to the activation of small subsets of the bases (i.e., a sparse set of the population) to encode different information; only a small subset of the coding outputs (feature maps or bases) are active for any given stimulus (input images), and different subsets are active for different stimuli. This ensures that the activation of different bases is a discriminator for different image data. In contrast, lifetime sparsity refers to the short frequency of

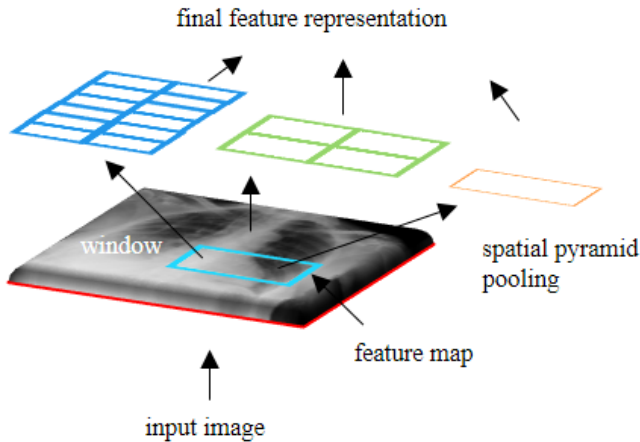


Fig 2. The spatial pyramid pooling layer on top of S-CKN.

Algorithm 1: EPLS [44]

Input: O, a, N

Output: T, c

1: $T = 0$

2: $O = (O - \min(O)) / (\max(O) - \min(O))$

3: **for** $n = 1$ **to** N_b

4: $O_j = O_{n,j} \forall j \in \{1, 2, 3, \dots, N_h\}$

5: $k = \operatorname{argmax}_j (O_j - c_j)$

6: $T_{n,k} = 1$

7: $a_k = a_k + N_n / N$

8: **end for**

9: Remap T to active/inactive values

k is the output that has to be activated in the n -th row of T and c_j is an accumulator that counts the number of times an output j has been selected.

activation of bases for different inputs (i.e., each base has a sparse lifetime); different bases are active very rarely and each activation has a high response. This ensures that the strong rare activations are indicators for high degree of information (the higher the information, the higher the entropy) about the underlying image data. A number of investigators have successfully applied sparsity to many situations including medical image segmentation and classification [7],[41],[42],[43]. Motivated by these findings, we hypothesise that incorporating sparsity into layerwise unsupervised pre-training could allow the extraction of more discriminative features for medical image data.

We formulated a layerwise unsupervised feature learning algorithm that efficiently enforces population and lifetime sparsity (EPLS) [44]. Our approach learns convolutional sparse features in reproducing kernel Hilbert space (RKHS), in contrast to the original EPLS algorithm by Romero et al. [44] that learns sparse features from decomposed raw image patches. The convolutional sparse features learned in the unified feature space are often more discriminative and therefore allow us to build more class-specific representations [45]. Furthermore, unlike the decomposed raw image patches, convolutional features preserve the relationships between neighbouring elements so as to learn local structures and reduce redundancy in the parameters [44, 46]. The learned parameters are used as initialisation points in CKNs learning (i.e., the initial value of $\theta = \{W, b\}$ of each layer). The algorithm iteratively creates a layer-specific sparse target of the input data and optimizes the dictionary by minimising the error between the output of the layer and the sparse target. The degree of sparsity is therefore controlled and learned differently at each layer. The parameters of the layer are then calculated as follows [44]:

$$\theta^l = \operatorname{arg min}_{\theta^l} \|O^l - T^l\|_2^2, \quad (7)$$

where $O^l \in \mathcal{R}^{N_b \times N_h}$ are the data vectors in RKHS, which are represented as a weighted combination of the training samples used to construct the kernel matrix at layer l , and T^l denotes the sparse target of the layer that addresses population and lifetime sparsity.

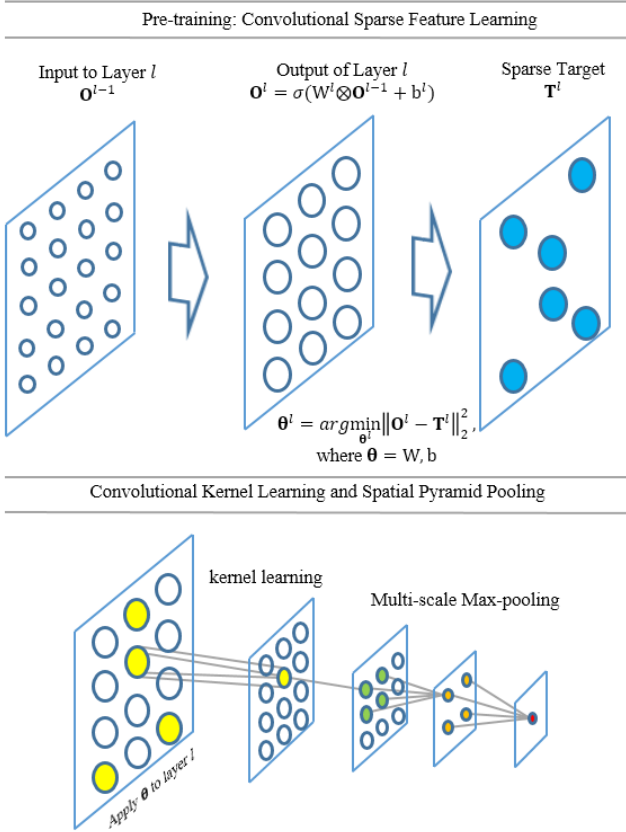


Fig 3. The architecture of our proposed algorithm.

Algorithm 1 is the pseudocode of the single layer EPLS derivation. Let us define \mathbf{O}_j as an element of row vector \mathbf{O} and denote \mathbf{O}^l as N_b output vectors of dimensionality N_h , where N_b is the size of mini-batch. Here, the b is the data related to a mini-batch and h is the total number of dimensions in \mathbf{O}^l . Starting with no activation in \mathbf{T}^l (line 1), input patches of \mathbf{O}^l are normalised between 0 to 1 (line 2). The algorithm iteratively processes a row vector \mathbf{O}_j of \mathbf{O}^l by selecting the k th element of the n -th row of \mathbf{O}^l that has the maximal activation value \mathbf{O}_k minus an inhibitor c_j (line 5). Here, the inhibitor is an accumulator that counts the number of times an output j has been selected, increasing its inhibition by N_h/N until reaching maximal inhibition, where N is the total number of training patches. This enforces the *lifetime sparsity* and prevents the selection of an output that has already been activated N_h/N times. The k th element of n -th row of target matrix \mathbf{T}^l is then activated as in line 6 (i.e., by assigning 1), considering *population sparsity*. The inhibitor is progressively updated and finally the output target is remapped to active and inactive values of corresponding non-linearity. The optimisation in relation to Equation 7 is performed using standard stochastic gradient descent (SGD) with adaptive learning rates [47].

E. Multi-layer Convolutional Kernel Networks

A CKN kernel can be learned in a hierarchical fashion for a deeper and potentially improved high-level semantic feature representation. Essentially: 1) the input feature map of layer $l + 1$ can be computed by applying the convolution operation, learned weights and biases to kernel maps from layer l ; 2)

EPLS is then used to learn initial sparse features used as a starting point of CKN learning; 3) a multi-layer CKN is learned in a feedforward manner, using a given input sub-patch of size S_z , and kernel parameters α and β for each layer. Fig 3 is an overview of our S-CKN framework.

F. The Spatial Pyramid Pooling (SPP) Layer

SPP is widely used in computer vision and has proven efficacy in representing the spatial layout of image features [48]. It partitions the image into multi-level regions and aggregates local features by taking spatial information into account. Hence, a number of researchers have successfully applied SPP to image classification [49], [50] and object detection [51]. Our assessment is that SPP can effectively characterise subtle geometric differences (e.g., size of similar bones or organs) in medical image data.

We added SPP as the last feature pooling layer to extract a final image representation that also captures subtle geometric variations. The outputs of the SPP layer are $p \cdot M$ dimensional vectors with M multi-level spatial bins (p is the filter size). We determined the window size of each pyramid level (n) based on the last feature maps ($x \times x$) generated from S-CKN, as $win = x/n$. We then pooled and aggregated the responses of each filter by selecting the maximum values (max pooling). This allowed us to minimise the computation cost and reduce over-fitting. Fig 2 and Fig 3 show a SPP layer combined with our S-CKN.

IV. EXPERIMENTAL SETUP AND RESULTS

A. IRMA X-ray Dataset

The Image Retrieval in Medical Application (IRMA) dataset comprises 14,410 gray-scale X-ray images with 193 hierarchical classes; the dataset has been used for many years for CAD development [24],[25]. IRMA is a challenging dataset because it contains images with irregular contrast, brightness, and artifacts. There is also high intra-class variability and inter-class similarity among the classes. We used the standard pre-defined training set of 12677 images and test set of 1733 images [25]. The images were annotated according to the IRMA coding system with four different axes, as described by Lehmann et al.



IRMA Code	1121-420-212-700
Technical Code	X-ray, Plain radiography, Overview Image
Directional Code	Other orientation, occipitofrontal
Anatomical Code	Facial cranium, eye area
Biological Code	Musculoskeletal system

Fig 4. Sample X-ray images (Face) and the corresponding labels from IRMA code.

[25]: 1) a technical code that describes imaging modality, 2) a directional code for imaging orientation, 3) an anatomical code for body region examined, and 4) a biological code for biological system examined. Fig 4 illustrates a sample X-ray image and the corresponding labels from the IRMA code.

B. ImageCLEF Dataset

We used the medical Subfigure Classification dataset used in the Image Conference and Labs of the Evaluation Forum (ImageCLEF) 2016 competition [52]. We used the standard pre-defined training set of 6776 images and test set of 4166 images from 30 different image modalities. Ground truth annotations are available for both image datasets. A detailed description of the datasets can be found in the ImageCLEF 2016 overview paper [52].

C. Experimental Setup

We evaluated our method in comparison to several unsupervised and supervised learning methods:

- conventional unsupervised feature learning approaches: SIFT+BoVW, Independent Component Analysis (ICA), and sparse coding [12]. We implemented the SIFT descriptor together with BoVW model (SIFT+BoVW). We used a patch size of 16x16 pixels with spacing of 8 pixels in the extraction of SIFT descriptors. We used the standard codebook size of 1000 [26]. The number of filters (i.e., weights) for the first layer of the ICA, and sparse coding was all set to 1600, which was consistent with other research [44].
- state-of-the-art unsupervised learning methods: SSAE [6, 13] and CKN [17]. The number of filters for the first layer of the SSAE was set to 1600, which was consistent with the conventional baselines above; We set the number of filters for the second layer to 1024. For the purpose of comparison, we trained the CKN using the same parameters as our proposed S-CKN (see Section IV.D).
- state-of-the-art supervised pre-trained CNNs (with natural images). We used the AlexNet [35], VGG [2], GoogLeNet [4], and ResNet [3], which have achieved high rankings in object recognition and localisation from the ImageNet Challenge. For all pre-trained CNNs models, the final fully-connected layers were used as the feature extractors.
- state-of-the-art supervised fine-tuned CNNs. We used the same models as in the pre-trained baselines above: AlexNet [35], VGG [2], GoogLeNet [4], and ResNet [3]. For medical image analyses, these fine-tuned CNNs have been shown to perform as well as fully trained CNNs or even outperform when there is limited training data [8],[9],[10]. All of the models were trained for 60 epochs with the IRMA dataset. We used a batch size of 128 and an initial learning rate of 10^{-4} . We used learning rate annealing, decaying the rate by a factor of 10 when the error plateaued.

All the networks (our S-CKN, the SSAE, the baseline CKN, and the fine-tuned CNNs) were trained with a GeForce GTX 1080 Ti GPU (11GB memory). It took 8 hours for our S-CKN to be trained with this GPU on a machine with Intel Core i7-

6800K 3.40 GHz (6 cores) processor. For the results of the supervised CNNs models with ImageCLEF dataset, we used the results reported in their papers [8].

We conducted medical image retrieval experiments on the IRMA dataset [26] and classification experiments on the ImageCLEF dataset [52]. For the medical image retrieval experiments, each of the test images was used as a query image and the training images were ranked according to the Euclidean distance from the query image. For quantitative comparisons, we used precision estimates at $Q = 1, 5, 10,$ and 30 as follows:

$$\text{Precision@Q} = \frac{\# \text{ relevant images in top } Q \text{ images retrieved}}{\# \text{ images of } Q \text{ retrieved images}} \quad (8).$$

For the classification experiments, we used the Top 1 accuracy (the correctness of the predicted label), which is the standard performance measure adopted in recent CNN studies for the classification of medical image modalities [8]. For all learned features, we used the setup of the multi-class linear SVM introduced by Yang et al. [49], who used a differentiable quadratic hinge loss so that the training could easily be done with simple gradient-based optimisation methods. We used LBFGS with a learning rate of 0.1 and a regularization parameter of 1, consistent with the parameters specified by Yang et al. [49].

D. Implementation Details

S-CKNs have four parameters that need to be determined for each layer: the size of sub-patch the coefficients α and β , and the pooling factor or filter size p . The parameters of our Gaussian kernel α and β are automatically determined for each layer. The coefficient β is set as the pooling factor divided by $\sqrt{2}$ consistent with the work reported by Mairal et al. [17]. The coefficient α can be set to be the 0.1 quantile of the distribution of pair-wise distances between sub-patches, as reported by Mairal et al. [17]. In our settings, the final results were insensitive to the use of smaller quantiles such as 0.01 and 0.001. This is also consistent with other research studies [18]. For the IRMA plain X-ray images, we adopted a two-layer architecture that was shown to perform better on gray-scale images [18]. We used the gradient map (defined in Section III.B) as the input of the initial layer of our architecture; the gradient map as input has been shown to perform better than raw patches [17]. Our parameter selection process searched within a restricted space to find the optimal values of the parameters, following other research studies [17]. We used values in the range 2 to 8 for sub-patch sizes and pooling factors

TABLE 1
FOR EACH LAYER, THE SUB-PATCH SIZE, SUB-SAMPLING FACTOR, AND THE NUMBER OF POOLING FACTOR ARE SHOWN. FOR INITIAL GRADIENT MAP, THE VALUES 16 INDICATES THE NUMBER OF ORIENTATIONS.

Dataset	Layer	Sub-patch Size	Sub-sampling Factor	Pooling Factor
IRMA	Layer 1	1x1	4	16
	Layer 2	3x3	4	1024
ImageCLEF	Layer 1	2x2	2	100
	Layer 2	2x2	4	800

of 100, 256, 512, 800 and 1024. For the ImageCLEF dataset, we used the same settings as the IRMA dataset but used raw patches instead of gradient maps as the input, as the raw patches performed better when working with RGB patches. We then empirically chose the remaining parameters as shown in Table 1. For the SPP layer, we used a 4-level spatial pyramid (1x1, 2x2, 3x3, 6x6) of 50 spatial bins in all of our experiments.

E. Results

The results of image retrieval experiments are shown in Table 2. We show sample results of the query and retrieval of varying structures in Fig 5. The query images are the shoulder of the scapulo-humeral joint (top row), shoulder of the acromioclavicular joint (middle row), and (bottom left) forearm (bottom

TABLE 2

AVERAGE IMAGE RETRIEVAL PRECISION ESTIMATES (%) AT Q = 1,5,10, AND 30 (BASED ON THE IRMA DATASET).

Type	Methods/ Average Q	1	5	10	30
Unsupervised	SIFT+BoVW	34.21	25.42	21.78	16.32
Unsupervised	SSAE (2 layers)	38.54	31.74	27.71	20.57
Unsupervised	ICA	33.92	26.10	22.42	16.69
Unsupervised	Sparse Coding	31.27	23.85	20.64	15.32
Supervised	Pre-trained AlexNet	37.91	30.46	26.72	20.90
Supervised	Pre-trained VGG-16	39.29	32.39	29.25	24.17
Supervised	Pre-trained VGG-19	38.83	32.46	29.54	24.20
Supervised	Pre-trained GoogLeNet -22	40.39	33.90	31.09	26.10
Supervised	Pre-trained ResNet-152	41.31	34.48	31.06	24.80
Supervised	Fine-tuned AlexNet	44.48	36.93	32.87	26.73
Supervised	Fine-tuned VGG-16	48.75	43.73	40.40	34.59
Supervised	Fine-tuned VGG-19	49.45	43.94	40.98	34.87
Supervised	Fine-tuned GoogLeNet	49.39	44.61	43.12	38.70
Supervised	Fine-tuned ResNet	47.20	41.66	39.11	34.56
Unsupervised	Our S-CKN	52.97	44.18	39.87	31.59

TABLE 3

TOP 1 IMAGE CLASSIFICATION ACCURACY (%) USING IMAGECLEF DATASET.

Type	Methods	Accuracy (%)
Unsupervised	Sparse Coding	57.08
Unsupervised	ICA	58.79
Unsupervised	SSAE (2 layers)	65.17
Supervised	VGG-like CNN (500 epochs) [55]	65.31
Unsupervised	Our S-CKN	70.99
Supervised	Fine-tuned AlexNet (100 epochs) with data augmentation [54]	77.55
Supervised	Modified GoogLeNet (60 epochs) with additional data [56]	81.03
Supervised	Ensemble of CNNs (50 epochs) with data augmentation [8]	82.48
Supervised	Fine-tuned ResNet-152 with additional data [56]	85.38

row), with artifacts including plates, screws and wires. The retrieved images are ranked by order of similarity from left to right (top 1 to 3).

Our approach had greater accuracy than other unsupervised feature learning algorithms as well as other pre-trained CNN models. Furthermore, our unsupervised S-CKN outperformed all the fine-tuned CNNs, achieving a top 1 precision of 52.97%. The fine-tuned GoogLeNet method achieved the best precision when considering the top 5, 10, and 30 retrieved images.

The results of image modality classification experiments are shown in Table 3. We compared our approach with several conventional unsupervised feature learning methods as well as the supervised image-based methods presented in the competition held in 2016. Our S-CKN had greater accuracy than other unsupervised approaches, achieving a top 1 accuracy of 70.99%. The second best unsupervised method was SSAE with an accuracy of 65.17%. The best performing supervised method was the fine-tuned ResNet-152 with an accuracy of 85.38%. Fig 6 shows how our sparsity-based pre-training improves the feature representation of medical images compared to other standard pre-training methods including random initialisation and the K-mean algorithm. We also show the improvement made by SPP.

V. DISCUSSION

A. Comparisons to Other Methods

Our findings show that our S-CKN outperforms other conventional unsupervised approaches and achieved competitive accuracy with the state-of-the-art supervised CNNs. We attribute this to: 1) the hierarchical kernel learning deriving semantically more meaningful image features (see Table 2 and 3); 2) sparse feature representation as part of layerwise pre-training, which extracts discriminative initial features for medical images (see Section V.B and V.C); and 3) spatial pyramid pooling that effectively characterises the local geometry information in medical image data (see Section V.C).

X-ray image retrieval – Our unsupervised S-CKN learns

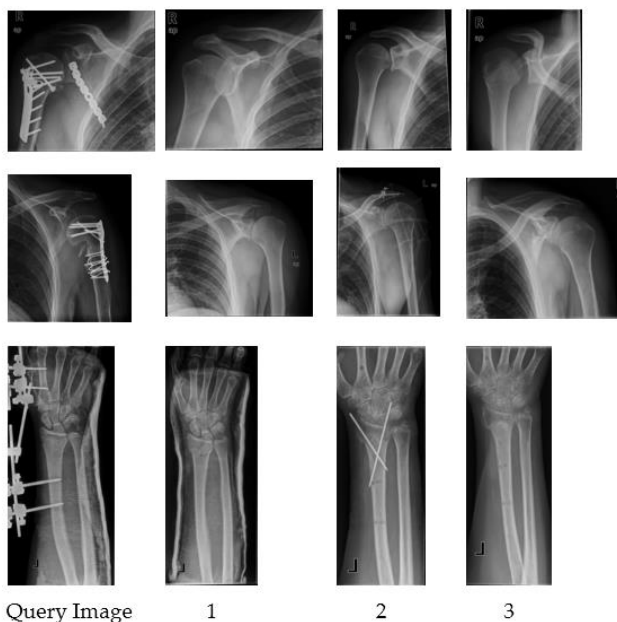


Fig 5. Sample results of query and retrieval of X-ray images using S-CKN.

and extracts data-specific features and achieved a high accuracy (52.97%) (see Table 2). Our results show that conventional unsupervised hand-crafted features such as SIFT coupled with BoVW model, sparse coding, and ICA could not extract discriminative features for X-ray images. The accuracy of pre-trained CNNs was lower than our method as these techniques extract features that are not tuned to a particular dataset or application, and as such have limited capacity to extract the most meaningful or discriminative features. The deeper network of pre-trained CNNs have higher accuracy (e.g., VGG-16 to ResNet-152 layers) and the fine-tuned GoogLeNet had the highest accuracy in top 5, 10, 30, and we attribute this to its network architecture exploiting the local sparse structure of a convolutional network [4]. Our method was designed to learn class-specific image features for better discrimination in an unsupervised fashion but this means it can be sensitive to subtle inter-class variations which is why accuracy drops faster as more subtly similar images are retrieved. For medical image retrieval applications, the five most similar images (i.e., top 5) for a query are commonly used for comparative analysis [53]. Our S-CKN achieved a competitive top 5 accuracy (44.18%), which was the second best after the fine-tuned GoogLeNet (44.61%).

Medical image modality classification – Our unsupervised S-CKN outperformed all other unsupervised approaches and achieved a comparable accuracy (70.99%) compared to all supervised CNNs that were part of the ImageCLEF 2016 challenge. Our results show that sparse coding and ICA could not learn and build discriminative image features, consistent with X-ray image retrieval results. Unlike sparse coding and ICA, the SSAE learned image features in a hierarchal manner and hence was the closest method to our approach. The top performing methods were all based on well-established supervised CNNs including AlexNet [54], VGG [55], GoogLeNet [56], and ResNet [56]. These CNNs were trained

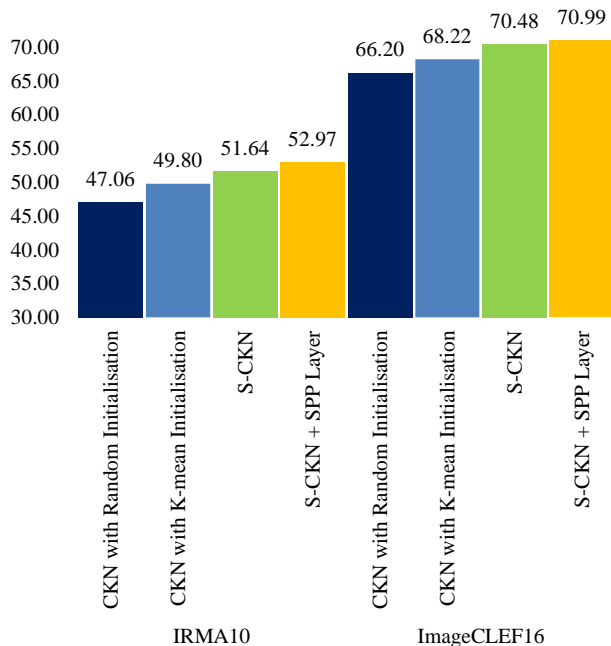


Fig 6. Top 1 average precision or accuracy of CKN with random and K-mean initialisation, and our Improved S-CKN with SPP.



Fig 7. The visualisation of learned weights by the first layer of the S-CKN using ImageCLEF dataset (gray-scale).

from scratch or fine-tuned with medical images to derive high level data specific features. The deeper CNNs also had higher accuracy than shallower CNNs (see Table 3). Our unsupervised S-CKN (accuracy of 70.99%) performed better than supervised VGG-like CNNs (65.31%) [55] with over 5% improvement in modality classification. While most of referenced methods used the same training data, the method by Koitka et al. [56] with the best performance in the competition, added extra data from additional sources.

The ImageCLEF dataset also contains different generic biomedical illustrations such as gene sequence or chemical structure and so, in comparison to the X-ray IRMA dataset, there were more diverse and complex variations in image characteristics. As a consequence, the overall performance of our approach was lower on the ImageCLEF dataset than the the IRMA dataset. Nevertheless, our method was able to derive discriminative medical image features from a variety of image modalities without reliance on labels, and its accuracy was better than that of supervised VGG-like CNNs [55].

B. Discovering the Structure of Medical Image Patches

Unsupervised learning is capable of discovering the underlying structure of image patches [57]. The learned weight parameters can be visualised using raw pixel data, and well-trained networks generally display some structure such as edges, lines, and ridges. The visualisation of the learned weights from the first layer of our S-CKN is shown in Fig 7. We used 400,000 image patches of size 12x12 and learned 256 filters [57]. Our S-CKN not only learned common structures such as lines and edges but also identified spatial patterns. Unlike the structure of natural image patches where lines, edges or blobs are dominant, our results show that the structure of medical image patches also contains spatially localised patterns, such as corners and sparse regions. These findings indicate that our S-CKN is able to learn the complex and diversified characteristics

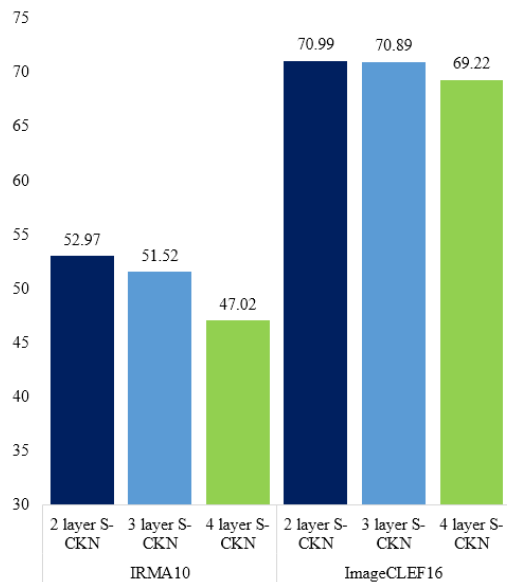


Fig 8. Results of retrieval and classification using deeper layers of S-CKN.

of medical image data.

C. The Role of Sparsity-based Pre-training and SPP Layer

The results from Fig 6 suggest that sparsity-based pre-training improves the feature representation of medical images compared to other standard pre-training methods including random initialisation and K-means algorithm. We attribute this to our robust pre-training scheme which provided good initialisation points for subsequent convolutional kernel learning. It acts as a form of regularisation that restricts parameters into certain spaces that are more discriminative for medical image data [15],[58]. The spatial pyramid pooling framework also improves feature representation in medical images (see Fig 6) through a multi-level spatial feature pooling technique that effectively characterises the local geometry information in the image data. To the best of our knowledge, this is the first research to couple unsupervised pre-training with unsupervised learning frameworks, which is dissimilar to conventional approaches that combine unsupervised pre-training with subsequent supervised learning [15],[59].

We also experimented with deeper architectures to further exploit the possibilities of extracting more high-level semantic image features. Our experiments using 3 and 4 layer S-CKN architectures did not result in any significant performance gain, which is consistent with other research [18] (see Fig 8).

We suggest that our unsupervised initialisation will benefit supervised learning approaches when there are limited labelled training data. We suggest that our S-CKN, when used to initialise a CNN for supervised fine-tuning, could potentially enable the derivation of semantically more meaningful representations of the image data than traditional CNN fine-tuning approaches that are initialised with natural images. The investigation of impact on fine-tuning is a substantial research study and it is something that we will pursue in future work. We suggest that our S-CKN could provide an important first step to accessing the large volume of unannotated data in medical imaging repositories. We note that compared to other

supervised CNNs, our S-CKN requires learning fewer parameters across fewer layers (two layers in this paper), and therefore, can be efficiently coupled with subsequent supervised learning approaches without a large computational cost.

D. Limitations

Although our approach improves the ability to learn feature representations of medical images without reliance on labelled data, some of the parameters (including sub-patch size or subsampling factor for each layer), must be empirically derived. In this study, our parameters were empirically determined by parameter search within a restricted space, which is a standard approach used in other research studies [17]. Generally, smaller subsampling factors and larger pooling factors (i.e., filter size) leads to better performance at the cost of increased computational complexity. Our results show that sparsity-based pre-training and SPP pooling consistently improved overall feature representation even when different parameters were used.

Our S-CKN is currently restricted to use an integral form of the Gaussian Radial Basis Function (RBF) kernel to approximate a kernel map (image feature representation in a RKHS). Other type of kernels or multiple kernels were not considered in this paper and we will explore such approaches in future work.

VI. CONCLUSION

In this paper, we proposed a new unsupervised sparsity-based feature learning technique to enable better characterisation of medical image data. Our layerwise pre-training technique, using convolutional sparse features, improves the learning outcome and feature representation in image retrieval and classification. We compared our approach to other unsupervised and supervised methods on two large public datasets and show that our approach is competitive with the state-of-the-art supervised CNNs. Our approach shows the feasibility of using large collections of unlabelled medical data to characterise medical image features and offers the opportunity to access the large volume of unannotated data that are available in medical imaging repositories. In future work we will explore the use of our S-CKN combined with subsequent supervised deep learning to optimise the ability derive semantically more meaningful representations of the image data.

REFERENCES

- [1] A. Kumar, J. Kim, W. Cai, M. Fulham, and D. Feng, "Content-Based Medical Image Retrieval: A Survey of Applications to Multidimensional and Multimodality Data," *Journal of Digital Imaging*, vol. 26, pp. 1025-1039, December 01 2013.
- [2] K. Simonyan and A. Zisserman, "Very deep convolutional networks for large-scale image recognition," *arXiv preprint arXiv:1409.1556*, 2014.
- [3] K. He, X. Zhang, S. Ren, and J. Sun, "Deep residual learning for image recognition," in *Proceedings of the IEEE Conference on Computer Vision and Pattern Recognition*, 2016, pp. 770-778.
- [4] C. Szegedy, W. Liu, Y. Jia, P. Sermanet, S. Reed, D. Anguelov, D. Erhan, V. Vanhoucke, and A. Rabinovich, "Going deeper with convolutions," in *Proceedings of the IEEE Conference on Computer Vision and Pattern Recognition*, 2015, pp. 1-9.

- [5] Q. V. Le, "Building high-level features using large scale unsupervised learning," in *Acoustics, Speech and Signal Processing (ICASSP), 2013 IEEE International Conference on*, 2013, pp. 8595-8598.
- [6] H.-C. Shin, M. R. Orton, D. J. Collins, S. J. Doran, and M. O. Leach, "Stacked autoencoders for unsupervised feature learning and multiple organ detection in a pilot study using 4D patient data," *Pattern Analysis and Machine Intelligence, IEEE Transactions on*, vol. 35, pp. 1930-1943, 2013.
- [7] E. Ahn, A. Kumar, J. Kim, C. Li, D. Feng, and M. Fulham, "X-ray image classification using domain transferred convolutional neural networks and local sparse spatial pyramid," in *2016 IEEE 13th International Symposium on Biomedical Imaging (ISBI)*, 2016, pp. 855-858.
- [8] A. Kumar, J. Kim, D. Lyndon, M. Fulham, and D. Feng, "An Ensemble of Fine-Tuned Convolutional Neural Networks for Medical Image Classification," *IEEE Journal of Biomedical and Health Informatics*, vol. 21, pp. 31-40, 2017.
- [9] N. Tajbakhsh, J. Y. Shin, S. R. Gurudu, R. T. Hurst, C. B. Kendall, M. B. Gotway, and J. Liang, "Convolutional Neural Networks for Medical Image Analysis: Full Training or Fine Tuning?," *IEEE Transactions on Medical Imaging*, vol. 35, pp. 1299-1312, 2016.
- [10] H.-C. Shin, H. R. Roth, M. Gao, L. Lu, Z. Xu, I. Noguees, J. Yao, D. Mollura, and R. M. Summers, "Deep convolutional neural networks for computer-aided detection: CNN architectures, dataset characteristics and transfer learning," *IEEE Transactions on Medical Imaging*, vol. 35, pp. 1285-1298, 2016.
- [11] L. Bi, J. Kim, E. Ahn, and D. Feng, "Automatic Skin Lesion Analysis using Large-scale Dermoscopy Images and Deep Residual Networks," *arXiv preprint arXiv:1703.04197*, 2017.
- [12] H. Lee, A. Battle, R. Raina, and A. Y. Ng, "Efficient sparse coding algorithms," in *Advances in neural information processing systems*, 2006, pp. 801-808.
- [13] G. E. Hinton, S. Osindero, and Y.-W. Teh, "A fast learning algorithm for deep belief nets," *Neural computation*, vol. 18, pp. 1527-1554, 2006.
- [14] V. Nair and G. E. Hinton, "Rectified linear units improve restricted boltzmann machines," in *Proceedings of the 27th international conference on machine learning (ICML-10)*, 2010, pp. 807-814.
- [15] D. Erhan, Y. Bengio, A. Courville, P.-A. Manzagol, P. Vincent, and S. Bengio, "Why does unsupervised pre-training help deep learning?," *Journal of Machine Learning Research*, vol. 11, pp. 625-660, 2010.
- [16] A. Romero, C. Gatta, and G. Camps-Valls, "Unsupervised deep feature extraction for remote sensing image classification," *IEEE Transactions on Geoscience and Remote Sensing*, vol. 54, pp. 1349-1362, 2016.
- [17] J. Mairal, P. Koniusz, Z. Harchaoui, and C. Schmid, "Convolutional kernel networks," in *Advances in Neural Information Processing Systems*, 2014, pp. 2627-2635.
- [18] M. Paulin, M. Douze, Z. Harchaoui, J. Mairal, F. Perronin, and C. Schmid, "Local convolutional features with unsupervised training for image retrieval," in *Proceedings of the IEEE International Conference on Computer Vision*, 2015, pp. 91-99.
- [19] J. Zhuang, J. Wang, S. C. Hoi, and X. Lan, "Unsupervised multiple kernel learning," *Journal of Machine Learning Research-Proceedings Track*, vol. 20, pp. 129-144, 2011.
- [20] A. Skodras, C. Christopoulos, and T. Ebrahimi, "The JPEG 2000 still image compression standard," *IEEE Signal processing magazine*, vol. 18, pp. 36-58, 2001.
- [21] A. Buades, B. Coll, and J.-M. Morel, "A review of image denoising algorithms, with a new one," *Multiscale Modeling & Simulation*, vol. 4, pp. 490-530, 2005.
- [22] R. Leahy and C. Byrne, "Recent developments in iterative image reconstruction for PET and SPECT," *IEEE transactions on medical imaging*, vol. 19, p. 257, 2000.
- [23] M. Lustig, D. Donoho, and J. M. Pauly, "Sparse MRI: The application of compressed sensing for rapid MR imaging," *Magnetic resonance in medicine*, vol. 58, pp. 1182-1195, 2007.
- [24] T. M. Lehmann, M. Gold, C. Thies, B. Fischer, K. Spitzer, D. Keysers, H. Ney, M. Kohnen, H. Schubert, and B. B. Wein, "Content-based image retrieval in medical applications," *Methods of information in medicine*, vol. 43, pp. 354-361, 2004.
- [25] T. M. Lehmann, H. Schubert, D. Keysers, M. Kohnen, and B. B. Wein, "The IRMA code for unique classification of medical images," in *Medical Imaging 2003*, 2003, pp. 440-451.
- [26] U. Avni, H. Greenspan, E. Konen, M. Sharon, and J. Goldberger, "X-ray categorization and retrieval on the organ and pathology level, using patch-based visual words," *Medical Imaging, IEEE Transactions on*, vol. 30, pp. 733-746, 2011.
- [27] M. Reza Zare, A. Mueen, and W. C. Seng, "Automatic classification of medical X-ray images using a bag of visual words," *Computer Vision, IET*, vol. 7, pp. 105-114, 2013.
- [28] A. Mueen, M. S. Baha, and R. Zainuddin, "Multilevel Feature Extraction and X-ray Image Classification," *Journal of Applied Sciences*, pp. 1224-1229, 2007.
- [29] Y. Anavi, I. Kogan, E. Gelbart, O. Geva, and H. Greenspan, "A Comparative Study for Chest Radiograph Image Retrieval using Binary, Texture, and Deep Learning Classification," in *37th Annual International Conference of the IEEE Engineering in Medicine and Biology Society (EMBC)*, 2015.
- [30] H. Müller, T. Deselaers, T. Deserno, P. Clough, E. Kim, and W. Hersh, "Overview of the ImageCLEFmed 2006 Medical Retrieval and Medical Annotation Tasks," in *Evaluation of Multilingual and Multi-modal Information Retrieval: 7th Workshop of the Cross-Language Evaluation Forum, CLEF 2006, Alicante, Spain, September 20-22, 2006, Revised Selected Papers*, C. Peters, P. Clough, F. C. Gey, J. Karlgren, B. Magnini, D. W. Oard, et al., Eds., ed Berlin, Heidelberg: Springer Berlin Heidelberg, 2007, pp. 595-608.
- [31] H. Müller, T. Deselaers, T. M. Deserno, J. Kalpathy-Cramer, E. Kim, and W. Hersh, "Overview of the ImageCLEFmed 2007 Medical Retrieval and Medical Annotation Tasks," in *Advances in Multilingual and Multimodal Information Retrieval: 8th Workshop of the Cross-Language Evaluation Forum, CLEF 2007, Budapest, Hungary, September 19-21, 2007, Revised Selected Papers*, C. Peters, V. Jijkoun, T. Mandl, H. Müller, D. W. Oard, A. Peñas, et al., Eds., ed Berlin, Heidelberg: Springer Berlin Heidelberg, 2008, pp. 472-491.
- [32] H. Müller, J. Kalpathy-Cramer, I. Eggel, S. Bedrick, S. Radhouani, B. Bakke, C. E. Kahn, and W. Hersh, "Overview of the CLEF 2009 Medical Image Retrieval Track," in *Multilingual Information Access Evaluation II. Multimedia Experiments: 10th Workshop of the Cross-Language Evaluation Forum, CLEF 2009, Corfu, Greece, September 30 - October 2, 2009, Revised Selected Papers*, C. Peters, B. Caputo, J. Gonzalo, G. J. F. Jones, J. Kalpathy-Cramer, H. Müller, et al., Eds., ed Berlin, Heidelberg: Springer Berlin Heidelberg, 2010, pp. 72-84.
- [33] H. Müller, A. G. S. de Herrera, J. Kalpathy-Cramer, D. Demner-Fushman, S. K. Antani, and I. Eggel, "Overview of the ImageCLEF 2012 Medical Image Retrieval and Classification Tasks," in *CLEF (online working notes/labs/workshop)*, 2012, pp. 1-16.
- [34] M. Abedini, N. C. F. Codella, J. H. Connell, R. Garnavi, M. Merler, S. Pankanti, J. R. Smith, and T. Syeda-Mahmood, "A generalized framework for medical image classification and recognition," *IBM Journal of Research and Development*, vol. 59, pp. 1:1-1:18, 2015.
- [35] A. Krizhevsky, I. Sutskever, and G. E. Hinton, "Imagenet classification with deep convolutional neural networks," in *Advances in neural information processing systems*, 2012, pp. 1097-1105.
- [36] L. Bo, X. Ren, and D. Fox, "Kernel descriptors for visual recognition," in *Advances in neural information processing systems*, 2010, pp. 244-252.
- [37] R. H. Byrd, P. Lu, J. Nocedal, and C. Zhu, "A limited memory algorithm for bound constrained optimization," *SIAM Journal on Scientific Computing*, vol. 16, pp. 1190-1208, 1995.
- [38] J. Ngiam, A. Coates, A. Lahiri, B. Prochnow, Q. V. Le, and A. Y. Ng, "On optimization methods for deep learning," in *Proceedings of the 28th International Conference on Machine Learning (ICML-11)*, 2011, pp. 265-272.
- [39] S. Li, H. Yin, and L. Fang, "Group-sparse representation with dictionary learning for medical image denoising and fusion," *IEEE Transactions on Biomedical Engineering*, vol. 59, pp. 3450-3459, 2012.
- [40] B. Willmore and D. J. Tolhurst, "Characterizing the sparseness of neural codes," *Network: Computation in Neural Systems*, vol. 12, pp. 255-270, 2001.
- [41] E. Ahn, J. Kim, L. Bi, A. Kumar, C. Li, M. Fulham, and D. Feng, "Saliency-based Lesion Segmentation via Background Detection in Dermoscopic Images," *IEEE Journal of Biomedical and Health Informatics*, 2017.
- [42] S. Zhang, Y. Zhan, and D. N. Metaxas, "Deformable segmentation via sparse representation and dictionary learning," *Medical Image Analysis*, vol. 16, pp. 1385-1396, 2012.
- [43] Z. Jiang, Z. Lin, and L. S. Davis, "Learning a discriminative dictionary for sparse coding via label consistent K-SVD," in *Computer Vision and Pattern Recognition (CVPR), 2011 IEEE Conference on*, 2011, pp. 1697-1704.

- [44] A. Romero, P. Radeva, and C. Gatta, "Meta-parameter free unsupervised sparse feature learning," *IEEE transactions on pattern analysis and machine intelligence*, vol. 37, pp. 1716-1722, 2015.
- [45] J. J. Thiagarajan, K. N. Ramamurthy, and A. Spanias, "Multiple Kernel Sparse Representations for Supervised and Unsupervised Learning," *IEEE Transactions on Image Processing*, vol. 23, pp. 2905-2915, 2014.
- [46] Y.-I. Boureau and Y. L. Cun, "Sparse feature learning for deep belief networks," in *Advances in neural information processing systems*, 2008, pp. 1185-1192.
- [47] T. Schaul, S. Zhang, and Y. LeCun, "No more pesky learning rates," *ICML (3)*, vol. 28, pp. 343-351, 2013.
- [48] S. Lazebnik, C. Schmid, and J. Ponce, "Beyond bags of features: Spatial pyramid matching for recognizing natural scene categories," in *Computer vision and pattern recognition, 2006 IEEE computer society conference on*, 2006, pp. 2169-2178.
- [49] J. Yang, K. Yu, Y. Gong, and T. Huang, "Linear spatial pyramid matching using sparse coding for image classification," in *Computer Vision and Pattern Recognition, 2009. CVPR 2009. IEEE Conference on*, 2009, pp. 1794-1801.
- [50] J. Wang, J. Yang, K. Yu, F. Lv, T. Huang, and Y. Gong, "Locality-constrained linear coding for image classification," in *Computer Vision and Pattern Recognition (CVPR), 2010 IEEE Conference on*, 2010, pp. 3360-3367.
- [51] K. E. Van de Sande, J. R. Uijlings, T. Gevers, and A. W. Smeulders, "Segmentation as selective search for object recognition," in *Computer Vision (ICCV), 2011 IEEE International Conference on*, 2011, pp. 1879-1886.
- [52] M. Villegas, H. Müller, A. G. S. de Herrera, R. Schaer, S. Bromuri, A. Gilbert, L. Piras, J. Wang, F. Yan, and A. Ramisa, "General Overview of ImageCLEF at the CLEF 2016 Labs," in *International Conference of the Cross-Language Evaluation Forum for European Languages*, 2016, pp. 267-285.
- [53] G. Quellec, M. Lamard, G. Cazuguel, B. Cochener, and C. Roux, "Wavelet optimization for content-based image retrieval in medical databases," *Medical Image Analysis*, vol. 14, pp. 227-241, 2010/04/01/2010.
- [54] A. Kumar, D. Lyndon, J. Kim, and F. Dagan, "Subfigure and multi-label classification using a fine-tuned convolutional neural network," in *CLEF2016 Working Notes. CEUR Workshop Proceedings, Évora, Portugal, CEUR-WS.org (September 5-8 2016)*.
- [55] D. Semedo and J. Magalhães, "NovaSearch at ImageCLEFmed 2016 subfigure classification task," in *CLEF2016 Working Notes. CEUR Workshop Proceedings, Évora, Portugal, CEUR-WS.org (September 5-8 2016)*.
- [56] S. Koitka and C. M. Friedrich, "Traditional feature engineering and deep learning approaches at medical classification task of ImageCLEF 2016," in *CLEF2016 Working Notes. CEUR Workshop Proceedings, CEUR-WS.org, Évora, Portugal (September 5-8 2016)*, 2016.
- [57] B. A. Olshausen and D. J. Field, "Emergence of simple-cell receptive field properties by learning a sparse code for natural images," *Nature*, vol. 381, p. 607, 1996.
- [58] D. Mishkin and J. Matas, "All you need is a good init," *arXiv preprint arXiv:1511.06422*, 2015.
- [59] T. Salimans and D. P. Kingma, "Weight normalization: A simple reparameterization to accelerate training of deep neural networks," in *Advances in Neural Information Processing Systems*, 2016, pp. 901-909.